AMERICAN SOCIETY FOR MICROBIOLOGY | Antimicrobial Agents and Chemotherapy®

MECHANISMS OF ACTION: PHYSIOLOGICAL EFFECTS

Dimeric Artesunate Glycerophosphocholine Conjugate Nano-Assemblies as Slow-Release Antimalarials to Overcome Kelch 13 Mutant Artemisinin Resistance

Yawei Du,[a,b] Carlo Giannangelo,[c] Wei He,[b] Gerald J. Shami,[a] Wenya Zhou,[b] Tuo Yang,[a] Darren J. Creek,[c] Con Dogovski,[a] Xinsong Li,[b] Leann Tilley[a]

[a]Department of Biochemistry and Pharmacology, Bio21 Molecular Science and Biotechnology Institute, The University of Melbourne, Parkville, Victoria, Australia
[b]School of Chemistry and Chemical Engineering, Southeast University, Nanjing, China
[c]Drug Delivery Disposition and Dynamics, Monash Institute of Pharmaceutical Sciences, Monash University, Parkville, Victoria, Australia

Xinsong Li and Leann Tilley contributed equally to this article. Author order was determined alphabetically.

ABSTRACT Current best practice for the treatment of malaria relies on short half-life artemisinins that are failing against emerging Kelch 13 mutant parasite strains. Here, we introduce a liposome-like self-assembly of a dimeric artesunate glycerophosphocholine conjugate (dAPC-S) as an amphiphilic prodrug for the short-lived antimalarial drug, dihydroartemisinin (DHA), with enhanced killing of Kelch 13 mutant artemisinin-resistant parasites. Cryo-electron microscopy (cryoEM) images and the dynamic light scattering (DLS) technique show that dAPC-S typically exhibits a multilamellar liposomal structure with a size distribution similar to that of the liposomes generated using thin-film dispersion (dAPC-L). Liquid chromatography-mass spectrometry (LCMS) was used to monitor the release of DHA. Sustainable release of DHA from dAPC-S and dAPC-L assemblies increased the effective dose and thus efficacy against Kelch 13 mutant artemisinin-resistant parasites in an *in vitro* assay. To better understand the enhanced killing effect, we investigated processes for deactivation of both the assemblies and DHA, including the roles of serum components and trace levels of iron. Analysis of parasite proteostasis pathways revealed that dAPC assemblies exert their activity via the same mechanism as DHA. We conclude that this easily prepared multilamellar liposome-like dAPC-S with long-acting efficacy shows potential for the treatment of severe and artemisinin-resistant malaria.

KEYWORDS artemisinin, glycerophosphocholine, malaria, nanoparticles, plasmodium

Malaria remains a leading threat to public health. A recent World Malaria Report (1), reports that 241 million new cases were recorded in 2020, resulting in more than 600,000 deaths. Children under the age of 5 continue to be among the most vulnerable, accounting for 77% of deaths in this period.

Artemisinin combination therapies (ACTs) are currently the front-line treatment option recommended by the World Health Organization for uncomplicated falciparum malaria, while parenteral or suppository artesunate (ARS) is the recommended treatment for severe malaria (2). ACTs are formulated to contain a fast-acting artemisinin-based drug, which functions to quickly reduce the parasite load, and a longer-acting partner drug to eliminate the remaining parasites. The pairing of drugs with different mechanisms of action is designed to slow or prevent the development of resistance.

Artemisinin, dihydroartemisinin (DHA), artemether (AM), and ARS (collectively referred to as artemisinins) belong to a class of sesquiterpene lactones incorporating an endoperoxide group that is critical for their activity (see Fig. 1a for examples) (3). Free heme, generated during hemoglobin digestion, activates artemisinins (4) by

Address correspondence to Leann Tilley, ltilley@unimelb.edu.au.

The authors declare no conflict of interest.

Received 21 October 2021
Returned for modification 17 November 2021
Accepted 24 March 2022
Published 13 April 2022

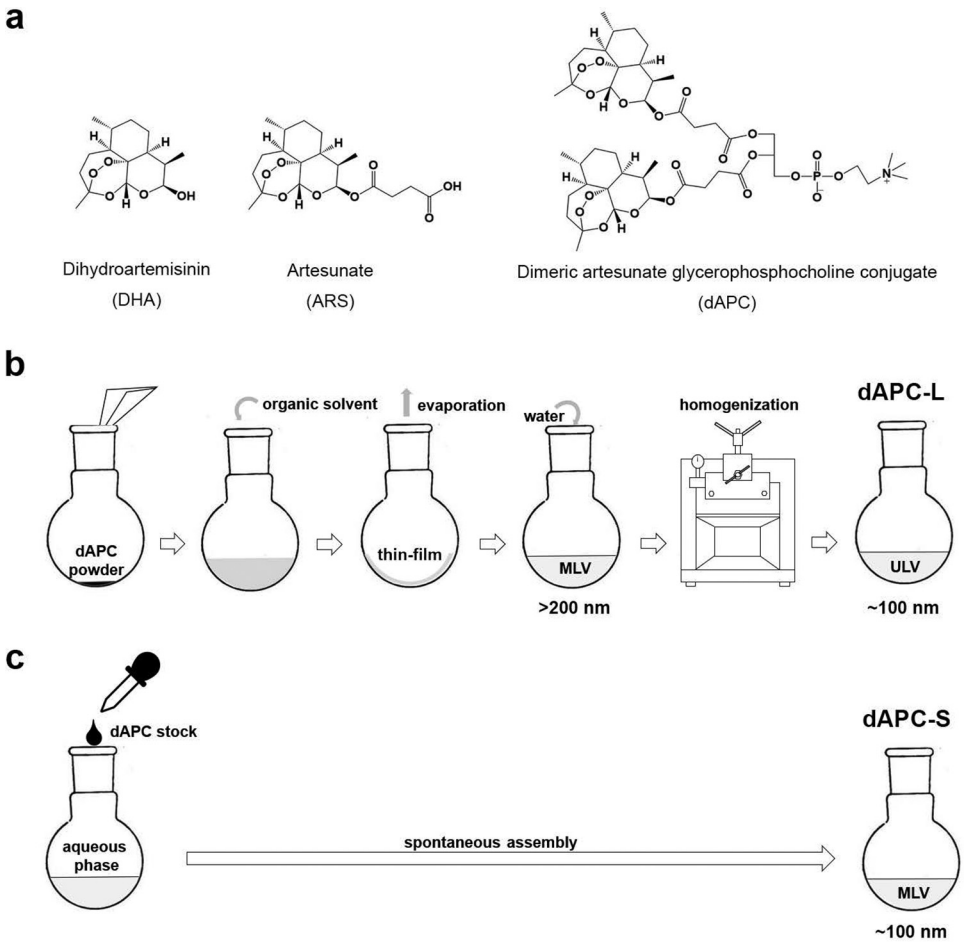

FIG 1 (a) Chemical structures of DHA, artemisinin, and dAPC. (b and c) Schematic representation of workflow for preparation of (b) dAPC-L and (c) dAPC-S. MLV, multilamellar vesicles; ULV, unilamellar vesicles. Vesicle sizes in nm are indicated.

opening the endoperoxide ring, leading to the production of radical species (5). The activated artemisinin intermediates react with susceptible (nucleophilic) groups within target molecules such as proteins, lipids, and heme (6–9). The resultant cellular damage eventually overwhelms the parasite's homeostasis systems (10, 11).

Different artemisinins exhibit different physicochemical and pharmacokinetic properties, tailored for different formulations and routes of delivery. DHA and AM exhibit poor solubility in water, and their administration is largely restricted to the enteral route and can show low (~20%) bioavailability (12, 13). An oil-based formulation of AM is also available for intramuscular delivery, but again, the bioavailability is low and variable (13, 14). ARS is sparingly water-soluble and is approved for intravenous, intramuscular, rectal, and oral delivery (15). Again, absorption of ARS is variable (16). Upon absorption into the bloodstream, both AM and ARS are converted to DHA (17). DHA exhibits a short *in vivo* half-life (~45 min), which necessitates a multidose treatment regimen in combination with a longer half-life partner drug to avoid parasite recrudescence (2). A novel formulation strategy for parenteral delivery of artemisinin-derivatives could provide an effective approach to overcome these limitations, especially for the treatment of severe malaria, which generally requires intravenous chemotherapy to ensure rapid antimalarial activity.

Unfortunately, the effectiveness of artemisinins has declined in Southeast Asia, manifesting as a delay in the clearance of parasites from the bloodstream following a standard 3-day ACT treatment regimen (18) and up to ~50% treatment failure in areas

with concomitant partner drug resistance (19, 20). Decreased sensitivity to artemisinins is associated with mutations in a Kelch domain protein (K13) (21). Worryingly, recent reports show mutations in K13 are appearing in Africa (22). Two recent studies suggest that K13 plays a role in hemoglobin internalization (23, 24). K13 mutants exhibit lower levels of K13 protein (23, 25). This partial loss of function of K13 leads to decreased hemoglobin uptake in the early ring stage, which in turn reduces the level of artemisinin activation, permitting parasite survival (23, 24). While early ring stage K13 mutant parasites are able to withstand exposure to short-lived artemisinins, prolonged drug exposure is expected to overcome the resistance mechanism (26, 27).

One possibility for improving the therapeutic potential of antimalarials and enhancing their tolerability, is via the use of slow-release nanoparticle formulations. Amphipathic molecules can be assembled to form micelles or liposomes in aqueous solution, and these structures may exhibit improved solubility, bioavailability, and plasma half-lives and reduced toxicity (28, 29). Nanoparticles based on naturally occurring lipids (typically, phosphatidylcholine, phosphatidylethanolamine, and cholesterol) or synthetic amphiphiles can be loaded with a drug of interest. For example, nanoparticle therapeutics, such as Doxil (liposomes) (30) and Genexol-PM (micelles) (31), are now employed in clinical tumor therapy. Nanoparticle assemblies containing antimalarials, such as chloroquine (32), ARS (33), primaquine (34), and DHA (35), have been described. However, conventional drug-loaded liposomes can suffer from poor and variable loading levels and poor stability (36–38). Recently, we and others have employed rational drug design strategies to modify existing drugs in order to stimulate their self-assembly and physical transformation into nanoparticles (39–41). This approach obviates the need for a carrier with a high loading rate to deliver the drug of interest. It also simplifies preparation and offers the possibility of slow-release formulations.

We previously described a dimeric artesunate glycerophosphocholine (GPC) conjugate (dAPC) as a novel antimalarial artemisinin-based prodrug (Fig. 1a) (42). The compound was synthesized by conjugating two ARS molecules to positions *sn*-1 and *sn*-2 of GPC. dAPC is an amphiphile, and previous studies used thin-film dispersion (42, 43) to assemble dAPC into liposome-like structures (dAPC-L). dAPC exhibited decreased cytotoxicity in a mouse leukemia cell line and a significantly extended *in vivo* half-life (~10 h) compared with ARS (~1.5 h) (42, 43). *In vitro* studies, employing a mixed-stage laboratory-adapted *Plasmodium falciparum* line, demonstrated the antimalarial activity of dAPC-L. Furthermore, dAPC-L exhibited improved activity compared with ARS for the treatment of *Plasmodium berghei*-infected mice (42).

In this study, we examine the properties of a spontaneously self-assembled dAPC preparation (dAPC-S) and explore the efficacy of the nano-assemblies against K13-mutant artemisinin resistant malaria parasites. We characterize the nano-assemblies using electron microscopy (EM) and dynamic light scattering (DLS). Liquid chromatography-mass spectrometry (LCMS) analysis shows that both dAPC-S and dAPC-L act as sustainable release reservoirs of DHA. This extends the effective dose of the active entity and increases the potency. As a consequence, dAPC-S and dAPC-L exhibit enhanced killing of artemisinin-resistant (K13 mutant) parasite lines compared to DHA. We conclude that easily prepared dAPC-S nano-assemblies have potential for development as long-acting formulations for the treatment of severe and artemisinin-resistant malaria.

RESULTS

Preparation of dAPC nanoparticles and characterization of size distribution and morphology. In this study, we compared spontaneously self-assembled dAPC nanoparticles, generated by direct suspension of dAPC in aqueous medium (dAPC-S; "Preparation of dAPC-L and dAPC-S"), with particles produced by dispersion of a dried thin-film (dAPC-L). Dynamic light scattering (DLS) of the samples (final concentration, 1 mM) revealed that the dAPC-S and dAPC-L preparations exhibit average diameters of 75 and 93 nm, respectively, with similar polydispersity (Fig. 2a).

Cryo-electron microscopy (cryoEM) revealed that dAPC-L particles are generally unilamellar, while dAPC-S particles are multilamellar (Fig. 2b). Analysis of particle sizes

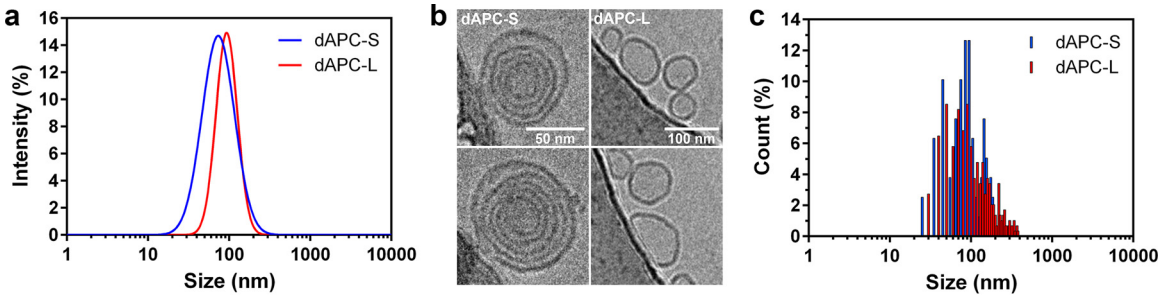

FIG 2 Characterization of dAPC nanoparticles. (a) Particle size distributions of dAPC-S (blue line) and dAPC-L (red line) analyzed by DLS. (b) CryoEM images of dAPC-S (left panels) and dAPC-L (right panels) (50 nm and 100 nm scale bars indicated); (c) particle size distributions of dAPC-S (blue bars) and dAPC-L (red bars) vesicles analyzed by cryoEM.

from micrographs confirmed the average sizes of approximately 85 and 90 nm, respectively, and again revealed the polydispersity of the samples (Fig. 2c).

dAPC assemblies act as sustainable release agents for DHA. To probe the stability of dAPC preparations relative to DHA during incubation in aqueous medium, we undertook LCMS analysis ("LCMS Analysis of the Release of DHA from dAPC") using high-resolution mass spectrometry. Quality control analysis of DHA samples confirmed that detection of DHA was in the linear range under the conditions of the assay (see Fig. S1 in the supplemental material). We note that DHA (in phosphate-buffered saline [PBS]) is rapidly degraded due to the presence of a lactol moiety, as reported previously (44). Upon incubation in PBS, or PBS plus 10% plasma, DHA is degraded with half-lives of 12.8 h and 9 h, respectively (Fig. 3a). Only 10% of the initial level remains after 24 h in PBS plus 10% plasma.

Quality control analysis of dAPC samples confirmed that detection of dAPC-S was in the linear range under the conditions of the assay (Fig. S2). During incubation of dAPC-S preparations in PBS, and PBS plus 10% plasma, dAPC is degraded with half-lives of 4.8 h and 9.4 h, respectively (Fig. 3b). The slower degradation in the presence of plasma suggests that protein-binding stabilizes dAPC. Interestingly, the analysis revealed that DHA is gradually released from the GPC conjugate, reaching a maximum after 12 h of incubation and then gradually declining (Fig. 3c). This analysis reveals that dAPC acts as an agent for the sustainable release of DHA. This slow-release behavior is expected to increase the potency of DHA by enhancing the effective dose of inhibitor to which the parasite is exposed (45). We therefore undertook a series of *in vitro* analyses to assess the relative activities of DHA and dAPC preparations.

A modified washing procedure is required to assess dAPC potency in pulsed *in vitro* exposure assays. The responses of *P. falciparum* cultures to artemisinins are best studied using inhibitor exposure times designed to mimic *in vivo* exposure (26, 45, 46). An important aspect of such assays is the efficient removal of the compounds from the culture wells, following the inhibitor pulse, to ensure that their activity is not overestimated (47). This is particularly important for more hydrophobic compounds that may

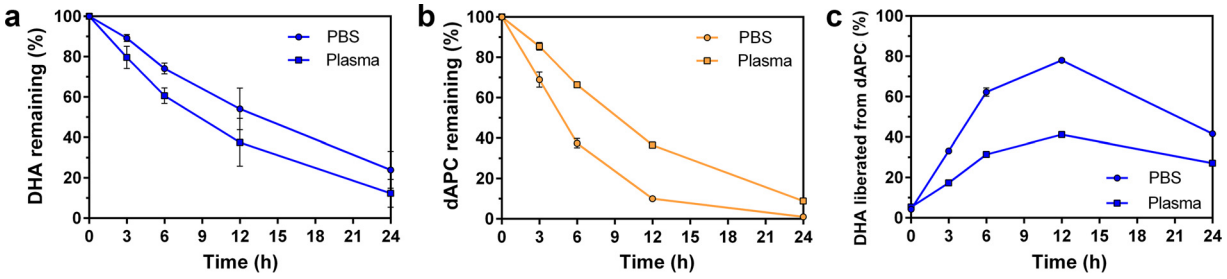

FIG 3 Chemical transformation of DHA and dAPC-S in aqueous media. DHA and dAPC-S were incubated in PBS (circles) and PBS + 10% plasma (squares) for the times indicated before quantitative analysis by HPLC and mass spectrometry. (a to c) DHA (a) was degraded, while loss of dAPC-S (b) was accompanied by release of DHA (c). The data represent the average of two independent experiments, each performed in duplicate. Error bars represent the standard error of the mean (SEM).

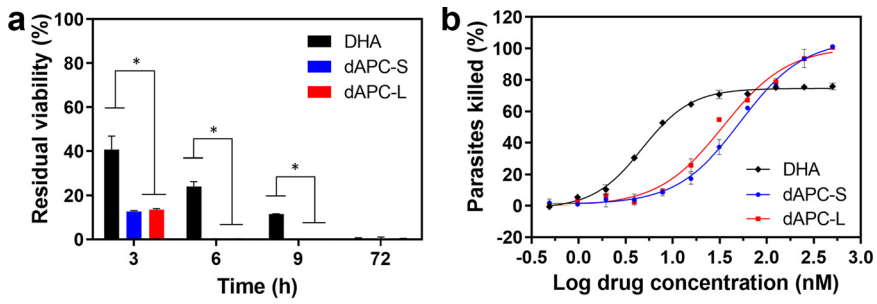

FIG 4 Antimalarial activity of DHA, dAPC-S, and dAPC-L in short-pulse exposure assays. (a) Ring-stage parasites (Cam3.II^{R539T}) were exposed to DHA (black), dAPC-S (blue), or dAPC-L (red) (500 nM) for the times indicated, and residual viability was measured in the following cycle. The data represent the average of 3 or more independent experiments, each in duplicate. The error bars represent the S.D. (b) Dose response curves for ring-stage Cam3.II^{R539T} parasites exposed to DHA (black, diamonds), dAPC-S (blue, circles), and dAPC-L (red, squares) for 6 h. The data are from an experiment performed in duplicate. The data are typical of three independent experiments. Error bars represent the range of values.

adhere to the plate well surface. Because the physicochemical properties of dAPC assemblies are different from those of DHA, it was important to establish a suitable inhibitor elimination (or wash) procedure.

Briefly, uninfected red blood cells (RBCs) were incubated for 3 h with a dilution series of the compounds, prior to four wash cycles. Cells were either maintained in the same plate or transferred to a fresh plate. Infected RBCs (Cam3.II^{rev}) were added, and viability was assessed in the next cycle (Fig. S3). While the standard wash protocol was sufficient to remove DHA, loss of parasite viability was observed at higher dAPC concentrations (500 to 1,000 nM) (Fig. S3a), indicating that residual compound remained in the wells. A modified protocol, involving transfer of RBCs to a fresh plate, was required to ensure elimination of residual inhibitor (Fig. S3b). This modified protocol was used for all further studies.

dAPC assemblies exhibit enhanced killing of artemisinin-resistant parasites in clinically relevant exposure assays. The K13 mutant line (Cam3.II^{R539T}) of *P. falciparum* exhibits decreased susceptibility to artemisinins at the ring stage of infection compared with the isogenic K13 wild-type line (Cam3.II^{rev}) (48), manifesting as residual viability following a short pulse exposure. Accordingly, following a 3-h exposure to DHA, the K13 mutant line exhibits a residual viability of 43% (Fig. 4a, Table S1), consistent with a previous report (47). dAPC-S and dAPC-L exhibit 50% lethal dose (LD_{50}) values for the 3-h pulsed exposure that are 1.3 to 3.6-fold higher than for DHA (Fig. S4b, Table S2). Nonetheless, exposure to dAPC-S and dAPC-L for 3 h at 500 nM, killed >85% of the K13 mutant parasites (Fig. 4a, Fig. S4a, Table S1). When the exposure time was increased to 6 h or 9 h, ~25% and 10%, respectively, of K13 mutant parasites remained viable after exposure to DHA, while no parasites survived exposure to dAPC-S and dAPC-L for the same period (Fig. 4a and b, Fig. S4b, Table S1). Thus, at anticipated exposures *in vivo*, both dAPC-S and dAPC-L would be expected to be more efficacious than DHA against K13 mutant parasites. We note that exposure to DHA for 72 h renders both the K13 wild-type and mutant lines nonviable (Fig. 4a, Table S1), as previously shown (47).

dAPC nanoparticles exhibit a time-dependent increase in potency and resist degradation. To better understand the differential potencies of dAPC-S, dAPC-L, and DHA, we examined their antimalarial activities following preincubation under different conditions. We assessed potency by exposing trophozoite-stage parasites (Cam3.II^{rev}) to the preincubated samples for 3 h. When applied without preincubation, DHA shows high antimalarial potency (LD_{50} for the 3-h pulsed exposure [LD_{50_3h}], 12 nM); however, its activity decreases rapidly upon incubation in RPMI 1640 (RPMI) medium or plasma-supplemented RPMI (Fig. 5a and b). For example, the LD_{50_3h} value increases to approximately 150 nM and 750 nM, respectively, following preincubation for 24 h (Fig. 5a and b). This represents a loss of ~90% and 98% of activity, respectively (Fig. S5c and d).

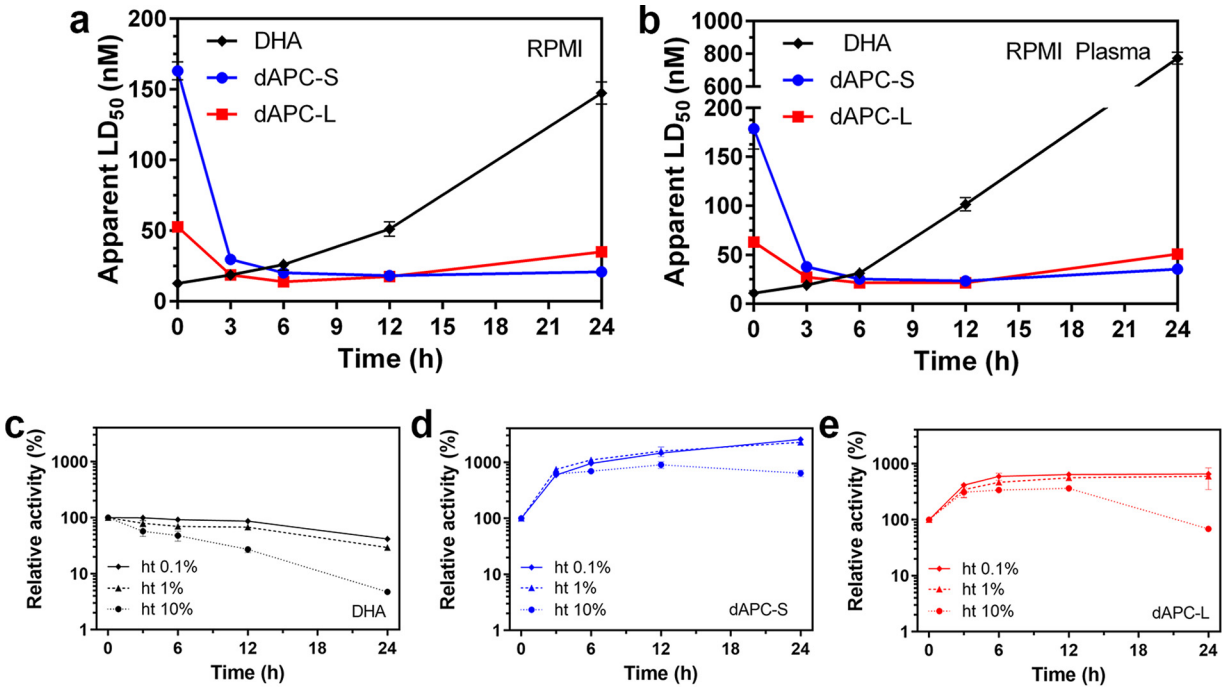

FIG 5 Effect of preincubation on antimalarial activity of DHA, dAPC-S, and dAPC-L. (a and b) DHA (black), dAPC-S (blue), and dAPC-L (red) were preincubated in (a) RPMI or (b) RPMI + 10% plasma for the indicated periods. The LD_{50} values were determined from a series of 10 dilutions in two independent experiments. Error bars represent the range of values for the two experiments. (c to e) DHA (c), dAPC-S (d), and dAPC-L (e) were preincubated in the presence of RBCs at 0.1% ht (unbroken line), 1% ht (dashed line) and 10% ht (dotted line) for the indicated periods. Remnant activity was assessed by exposing infected RBCs to the preincubated compound samples for 3 h, with viability assessed in the next cycle. Dose response curves were generated, and relative activity was estimated compared with activity prior to preincubation, defined as LD_{50} (time = 0)/LD_{50} (time = *t*) multiplied by 100. The remnant activity values are determined from a series of 10 dilutions in two independent experiments. Error bars represent the range of values for the two experiments.

This loss of activity is consistent with the previously reported poor stability of DHA under culture conditions (49, 50).

Heat inactivation of the plasma did not prevent loss of DHA activity (Fig. S6), suggesting that the deactivation is not mediated by serum esterases. The loss of potency was less dramatic in PBS or PBS plus plasma (Fig. S5a and b) than in RPMI (Fig. S5c). This suggests that inactivation is due to chemical decomposition (51), exacerbated by RPMI components, such as trace iron in the presence of the glutathione reducing agent in RPMI. Accordingly, we showed that addition of extra iron exacerbated the loss of activity (Fig. S7).

In the absence of preincubation, dAPC-L and, particularly, dAPC-S (Fig. 5a and b), show lower initial levels of potency than DHA (IC_{50_3h} values of ~50 and ~150 nM, respectively). However, the potency increased 3- to 10-fold upon incubation in RPMI medium or plasma-supplemented RPMI (Fig. 5a and b, Fig. S5c and d). The IC_{50_3h} values for both compounds decreased to 10 to 20 nM following incubation for 12 h, and the preparations retained good potency following incubation for 24 h (Fig. 5a and b). Interestingly, the initial increase in potency upon incubation of dAPC-S in PBS, and PBS plus plasma (Fig. S5a and b), correlates very well with the estimated increase in DHA due to release from dAPC (Fig. 3c).

Instability due to ferrous iron (and heme released from hemoglobin) in uninfected RBCs is considered to be a major contributor to the very short *in vivo* half-life of DHA (50, 52). In this work, we examined the effect of incubating DHA and the dAPC nanoparticle preparations at increasing hematocrit (ht) levels. Exposure of DHA to a 10% suspension of RBCs in PBS for 24 h reduced the level of activity by ~94% (Fig. 5C, Fig. S5e). In contrast, upon incubation with a 10% suspension of RBCs in PBS, dAPC-S and dAPC-L exhibited initial gains in potency and remained more potent (dAPC-S) or retained close to 100% of the initial activity (dAPC-L), even after 24 h of incubation

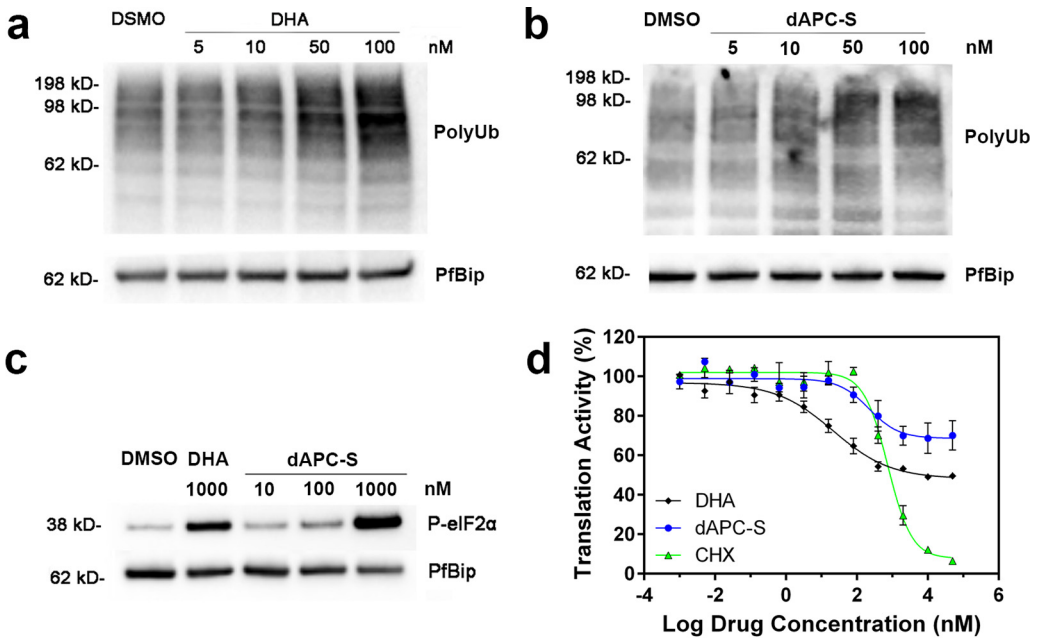

FIG 6 Disruption of proteostasis underpins parasite killing by dAPC nanoparticles. (a and b) Trophozoite-stage infected RBCs (Cam3.II^{rev}) were incubated with carrier (0.1% DMSO) or increasing concentrations (indicated) of DHA (a) or dAPC-S (b) for 90 min. Extracts were probed with antiserum recognizing polyubiquitinated proteins. *Pf*BiP is a loading control. The data represent matched blots from the same day. Blots from three additional experiments are presented in Fig. S8. (c) Lysate from trophozoite-stage parasites exposed to carrier, DHA, and dAPC (concentrations indicated) for 3 h were analyzed by Western blotting for phosphorylated-eIF2α. *Pf*BiP is a loading control. Blots from three additional experiments are presented in Fig. S8. (d) Protein translation was measured in trophozoite-stage parasites (Cam3.II^{rev}) that were exposed to increasing concentrations of DHA (black, diamonds), dAPC-S (blue, circles), or cycloheximide (green, triangles) for 60 min before incorporation of *O*-propagyl-puromycin (OPP). Cultures were incubated for a further 120 min before parasites were harvested for determination of OPP incorporation. The data represent the average of two technical replicates. Error bars represent the range of the individual values. A replicate data set is presented in Fig. S9.

(Fig. 5d and e, Fig. S5f and g). Thus, the sustainable release of DHA from dAPC means that it is protected from rapid degradation, likely enhancing its *in vivo* exposure and providing the superior *in vivo* efficacy of the nanoparticle preparations (42).

dAPC assemblies exert their activity via the same mechanism as DHA. Artemisinins exert their activity by causing widespread protein damage, leading to a build-up of polyubiquitinated proteins that eventually overwhelms the parasite's stress response and causes cell death (10). While it seems likely that dAPC preparations exert their activities via a similar mechanism, this has not been formally demonstrated. Based on a previous report (26), we exposed trophozoite stage cultures of *P. falciparum* (Cam3.II^{rev}) to a range of concentrations of DHA or dAPC-S for 1.5 h (Fig. 6). Parasite proteins were isolated and the level of polyubiquitinated proteins analyzed by Western blotting (Fig. 6a and b, Fig. S8). Exposure of parasites to either DHA or dAPC resulted in a concentration-dependent increase in protein ubiquitination.

Accumulation of unfolded proteins triggers endoplasmic reticulum (ER)-stress, leading to eIF2α (α subunit of eukaryotic initiation factor 2) phosphorylation and partial inhibition of protein translation (23, 53). We exposed trophozoite-stage parasites to different compounds for 3 h. dAPC-S exposure triggered eIF2α phosphorylation in a dose-dependent manner (Fig. 6c, Fig. S8), reaching a level similar to that achieved upon exposure to DHA (1 μM) (Fig. 6c).

To monitor protein translation efficiency, we used a flow cytometry-based assay to measure the level of incorporation of a fluorescent puromycin derivative, extending a previously published method (54). Parasites were exposed to DHA for 1 h, before addition of *O*-propargyl-puromycin (OPP) for a further 2 h to measure the translation level. DHA exposure (for a total period of 3 h) inhibited translation to a maximal level of 50

to 60% (Fig. 6d, Fig. S9), in agreement with a previous report (23). dAPC-S also inhibited protein translation, reaching a maximal level of 30 to 50% inhibition (Fig. 6d, Fig. S9). The well-characterized ribosome-targeted inhibitor cycloheximide also inhibited protein translation in this assay format, with an IC_{50} value of 0.7 μM (Fig. 6d, Fig. S9), in agreement with a previous report (23). Taken together, the data support the suggestion that dAPC kills parasites in a manner similar to DHA.

DISCUSSION

In a previous study, we reported a novel artemisinin derivative, dAPC, that mimics the structure of natural phosphatidylcholines (42). Using a classic liposome preparation protocol, dAPC was assembled into unilamellar vesicle (ULV) liposomes (dAPC-L) without any other excipients. dAPC exhibited inherently full drug-loading and significantly improved *in vivo* half-life and efficacy *in vitro* and *in vivo* (42). Here, we aimed to understand the molecular basis for the enhanced potency and to develop more practical formulations suitable for transfer to the clinic.

In contrast to traditional liposomal preparations, the self-assembly process described here requires no specialist equipment. Amphiphilic compounds spontaneously self-assemble to form nanoparticles that can take the form of micelles, liposomes, or liquid crystals (55). Using cryoEM and DLS analyses, we showed that dAPC-S self-assembles into multilamellar vesicles (MLV) with a similar size distribution to dAPC-L in the ULV form.

Artemisinins are thought to kill malaria parasites by damaging proteins and membranes (10). In order to exert their activity, artemisinins must first be activated by ferrous iron attack on the peroxide oxygen atom to form an alkoxy radical that undergoes β-scission to form a secondary carbon-centered free radical (56). The same chemical reactions also underpin the instability of artemisinins in medium containing a source of reduced iron and contribute to the rapid clearance from the bloodstream *in vivo* (44).

The very short *in vivo* half-lives (0.5 to 1.5 h) mean that a single treatment with clinically used artemisinins does not deliver sufficient exposure (to activated inhibitor) to kill all parasites, particularly in the ring stage of development when the flux of hemoglobin digestion is low (26, 45). Recent work shows that mutations in the Kelch 13 (K13) gene confer decreased artemisinin sensitivity by further dampening hemoglobin endocytosis (23, 24). As a consequence, a substantive proportion of the population of ring-stage K13 mutant parasites are not killed by clinically relevant artemisinin exposures. Modeling studies have predicted that artemisinin derivatives that exhibit slower degradation rates, which increases the duration of exposure to activated artemisinin, would possess superior ability to kill K13 mutant parasites (45).

In this work, we used chromatographic separation and mass spectrometry to assess the fate of dAPC and DHA during incubation in aqueous medium. DHA is degraded rapidly, even in PBS, in agreement with previous reports (49, 50). Decomposition products can include deoxyartemisinin (51), isomeric decomposition products, and several other end products dependent on the reaction system (3, 57, 58). Interestingly, dAPC is also transformed during incubation, but in this case, it acts as a sustainable release reservoir for DHA. The endoperoxide bond appears to be protected from degradation in the context of the GPC conjugate, and the sustainable release profile effectively extends the exposure to DHA.

We examined the ability of DHA, dAPC-S, and dAPC-L to inhibit the growth of cultures of wild-type and K13 mutant *P. falciparum*. K13 mutant parasites exhibited much lower residual viability when exposed to dAPC-S or dAPC-L than to DHA. This effect is particularly dramatic for exposure pulses of 6 or 9 h, which mimic the longer *in vivo* half-life of dAPC (42). We anticipate that this enhanced activity is due to the higher effective dose of DHA (i.e., longer exposure time) provided by the slow-release mechanism, such that the proteotoxic stress reaches the toxic level (59).

We undertook a more detailed analysis of the factors that underpin the differential degradation of DHA and dAPC in different aqueous media. Following incubation for 24 h at 37°C in the presence of plasma-containing culture medium, the antimalarial

activity of DHA was completely ablated, consistent with previous reports (57). Our detailed analysis showed that the degradation was relatively slow in PBS ($t_{1/2}$ ~12 h) but increased in culture medium (half-life [$t_{1/2}$], ~6 h) and was very rapid in plasma-supplemented culture medium ($t_{1/2}$ ~3 h). Incubation in the presence of an increasing hematocrit of RBCs also caused rapid degradation of DHA, likely due to the ferrous iron or heme present at low levels in the RBC cytoplasm (60).

In contrast, the potency of dAPC-S increases upon incubation in each of the media examined, reaching a maximal level at ~12 h and then gradually declining. Comparison with the quantitative analysis of the fate of dAPC in PBS, and PBS plus plasma, confirmed that the incubation-induced increase in potency is very well correlated with the increase in DHA concentration, due to release from dAPC. Similarly, the subsequent loss of potency (after >12 h of incubation) correlates with the decrease in DHA concentration, due to chemical degradation.

The ability of reduced iron to attack the endoperoxide bond of artemisinins is decreased if the bond is less accessible (61, 62). We propose that the much lower susceptibility of dAPC to chemical degradation is due to burying reactive groups in the center of the bilayer of the dAPC assemblies (or potentially upon binding to serum lipoproteins), which may protect against degradation. The sustainable release of DHA from dAPC nanoparticles provides a drip-feed of DHA.

As expected, dAPC assemblies appear to exert their activity via the same mechanism as DHA. Upon exposure to dAPC, parasites display the hallmarks of ER stress, which include protein polyubiquitination, eIF2α phosphorylation, and consequent downregulation of protein synthesis. The longer *in vivo* half-life time of dAPC and gradual conversion to DHA means that parasites will be subjected to protein damage for a longer period that eventually overwhelms the parasite's defense system.

The excellent activity of dAPC assemblies suggests that more complex formulations may not be needed. The easy to prepare, relatively low-cost dAPC-S formulation may be sufficient. dAPC nano-assemblies offer clear advantages for parenteral and intramuscular routes of delivery for treatment of artemisinin-resistant (K13 mutant) malaria; however, we note a limitation of dAPC with respect to oral formulations, as it would be expected to undergo rapid conversion to DHA at the pH of the stomach. Further research could explore the possibility of different linkages that would be more acid resistant.

Conclusions. In summary, we have examined two different methods for preparation of dAPC nano-assemblies. A careful analysis of the behavior of these preparations in an *in vitro* culture system revealed that the endoperoxide group is protected from chemical degradation until the DHA is released from the conjugate. With further development, dAPC-S holds promise as a much-needed stable injectable formulation with enhanced activity against artemisinin-resistant parasites.

MATERIALS AND METHODS

Materials. 1,1′-Carbonyldiimidazole (CDI) and 1,8-diazabicyclo-[5.4.0]-undec-7-ene (DBU) were supplied by Aladdin Bio-Chem Technology Co., Ltd. (Shanghai, China). L-α-glycerophosphocholine (GPC) was provided by Fushilai Medicine & Chemical Co., Ltd. (Changshu, China). Dihydroartemisinin (DHA) was purchased from Tokyo Chemical Industry (TCI) Co., Ltd. (Tokyo, Japan). All organic solvents used in this work were analytical or higher grade. Tween 20, Tris(3-hydroxypropyltriazolylmethyl)amine (THPTA), Triton X-100, propidium iodide (PI), and dimethyl sulfoxide (DMSO) were purchased from Sigma-Aldrich (St. Louis, MO). RPMI 1640 (catalog [cat.] no. 21870076) and AlbuMAX II (cat. no. 11021045) were purchased from Life Technologies (Carlsbad, CA). Human pooled serum and red blood cells (RBCs) (O^+) were supplied by the Australian Red Cross Blood Service (Melbourne, Australia). cOmplete protease tablets (cat. no. 05892791001) were purchased from Roche (Welwyn Garden City, UK). Anti-ubiquitin antibody (cat. no. 3933S) and anti-phospho-eIF2α (Ser51) antibody (cat. no. 9721S) were purchased from Cell Signaling Technology (Danvers, MA). Anti-*Pf*BiP antibody was kindly provided by Alan Cowman, The Walter and Eliza Hall Institute (Melbourne, Australia). Goat anti-rabbit IgG antibody (cat. no. A0545) was purchased from Sigma-Aldrich, and goat anti-mouse IgG antibody (cat. no. AP127P) was purchased from Merck (Darmstadt, Germany). SeeBlue Plus2 prestained protein standards (cat. no. LC5925), Bolt Bis-Tris 4 to 12% polyacrylamide gels (cat. no. NW04122BOX), Bolt lithium dodecyl sulfate (LDS) sample loading buffer (cat. no. B0008), morpholineethanesulfonic acid (MES) running buffer (cat. no. B0002), and sample reducing agent (cat. no. B0009) were purchased from Life Technologies. Pierce ECL Western blotting substrate (cat. no. 32106) and SYTO 61 red fluorescent nucleic acid stain (SYTO61) (cat. no. S11343) were purchased from Thermo Fisher Scientific. *O*-propargyl-puromycin (OPP) (cat. no. 1407-5) and Alexa Fluor 488 azide (cat. no. 1275-1) were purchased from Click Chemistry Tools (Scottsdale, AZ).

Synthesis of dAPC. The dAPC was synthesized by a heterogeneous esterification reaction as reported previously (42). Briefly, ARS (1.0 mmol) was activated using CDI (1.5 mmol) in anhydrous dimethyl sulfoxide (DMSO; 20 mL) for 2 h. GPC (0.4 mmol) and DBU (4.0 mmol) were mixed in DMSO (10 mL) for 15 min and then added to the reaction mixture and stirred overnight. The reaction mixture was separated using a traditional silica gel chromatographic column with eluent A (CH_2Cl_2/CH_3OH, 5/1, vol/vol) and then eluent B ($CH_2Cl_2/CH_3OH/H_2O$, 65/25/4, vol/vol/vol). The desired fractions were vacuum dried, producing the crude product as a faint yellow solid. The crude product was further purified by high-performance liquid-phase column chromatography using a C_{18} column (NS4000; Hanbon Sci. & Tech. Co., Huai'an, China) with bound material eluted in $CH_2Cl_2/CH_3OH/H_2O$ (65/25/4, vol/vol/vol). The desired fractions were vacuum dried, producing a white solid with a purity of 97.3% (yield, ~40%).

Preparation of dAPC-L and dAPC-S. The dAPC liposomes (dAPC-L) were prepared by thin-film dispersion as described previously (Fig. 1b) (42). Briefly, dAPC (10 mg, 10 μmol) powder was dissolved in 50 mL chloroform and placed in a 100-mL round-bottom flask. Rotary evaporation under reduced pressure at 30°C was employed to produce a thin film. A suspension was created by resuspending dAPC in 10 mL PBS (pH 7.4). The sample was maintained in a round-bottom flask at 40°C with shaking for 10 min to produce liposomes with a final concentration of 1 mM. LCMS analysis revealed that the preparation contains a small level (~4%) of DHA. The liposome suspension was homogenized by several passages through a Millipore Millex-HV 0.45-μm filter. To prepare dAPC-S (Fig. 1c), dAPC was dissolved in DMSO to 100 mM and slowly added into PBS to achieve a final dAPC concentration of 1 mM. The suspension was incubated for 30 min at room temperature with gentle mixing. LCMS analysis revealed that DHA represents ~4% of the preparation.

Dynamic light scattering. Nanoparticle size was measured using dynamic light scattering (DLS) on a Zetasizer Nano ZS 90 instrument (Malvern Instruments Ltd.). Nanoparticle samples were analyzed at a final concentration of 1 mM. Measurements were taken over a 50-s time period with 10 replicates at 20°C. The samples were illuminated with a 4-mW He-Ne laser operating at 633 nm, and experiments were conducted at a scattering angle of 173 degrees. The built-in analysis software was used to determine average particle hydrodynamic sizes.

CryoEM sample preparation and imaging. The dAPC (4 μL of 1 mM stock in PBS) was applied to glow-discharged Quantifoil Cu 1.2/1.3 or UltrAuFoil 1.2/1.3 on a 300-mesh grid. Samples were vitrified in liquid ethane using a Vitrobot Mark IV (Thermo Fisher Scientific) plunge freezer set to 22°C with 100% relative humidity. Grids were blotted with a blot time of 4 s, blot force of −1, and wait time of 30 s. The vitrified samples were transferred to a Gatan 626 cryo transfer holder and imaged using a Tecnai G2 TF30 (FEI) field-emission transmission electron microscope operating at 200 kV.

LCMS analysis of the release of DHA from dAPC. DHA and dAPC-S (100 μM) were incubated in PBS and PBS plus 10% plasma at 37°C for 3, 6, 9, 12, and 24 h before LCMS analysis. Samples were analyzed using high-resolution mass spectrometry (Q Exactive, Thermo Fisher) coupled with a Dionex Ultimate 3000 ultra high-performance liquid chromatography (UHPLC) system (Thermo Fisher). Analytical separation was performed on a 100 mm by 2.1 mm, 2.7-μm Ascentis Express C_8 or 150 mm by 2.1 mm, 1.9- μm Thermo Fisher Hypersil GOLD C_{18} reversed phase column, with a guard column of the same material (Sigma-Aldrich). Compounds were eluted using a binary gradient solvent system consisting of 20 mM ammonium formate, pH 6 (solvent A), and acetonitrile (ACN) (solvent B). The gradient profile was as follows: 0 to 4 min, 20 to 98% B; 4 to 6.5 min, 98% B; 6.5 to 7 min, 98 to 15% B and 7 to 11 min, 15% B. The compounds of interest eluted between 1.5 and 5 min at a flow rate of 0.4 mL/min. Mass spectrometry was performed as a full scan acquisition in polarity switching mode, with the following settings: resolution, 35,000; AGC target, 1×10^6; *m/z* range, 100 to 1,250; sheath gas, 34; auxiliary gas, 13; spare gas, 2; probe temperature, 120°C; and capillary temperature, 300°C. For positive ionization mode, the spray voltage was set at +4 kV and the S-lens voltage at +50 V. For negative ionization mode, the spray voltage was set at −3.5 kV and the S-lens voltage at –50 V. Targeted detection based on accurate mass (± 3 ppm) and retention time, and integration of LCMS peak areas for the analytes of interest, was performed using Thermo Xcalibur Quan Browser (version 4.2 SP1).

Parasite culture and tight synchronization. The *P. falciparum* lines employed in this study were propagated in O^+ human RBCs (Australian Red Cross Blood Service) in complete culture medium (CCM) defined as RPMI 1640 (RPMI), supplemented with GlutaMAX, 25 mM HEPES (Thermo Fisher), 5% (vol/vol) human serum (Australian Red Cross Blood Service), 0.25% (wt/vol) AlbuMAX II (Life Technologies), 10 μM D-glucose, 22 μg mL^{-1} gentamicin, and 0.5 mM hypoxanthine, and incubated at 37°C in an atmosphere of 1% O_2, 5% CO_2, and 94% N_2. Cultures were monitored by Giemsa staining of methanol-fixed blood smears. Culture medium was replaced at least every 48 h, and parasitemia (pt) was maintained below 5% to ensure health of the cultures. Parasites were synchronized by two sorbitol treatments as described previously (26, 45), yielding ring- (0 to 5 h postinvasion [p.i.]) or trophozoite-stage (25 to 30 h p.i.) parasites for use in experiments. The *P. falciparum* lines used in this study, Cam3.II^{rev} (K13 wild type) and Cam3.II^{R539T} (K13 mutant) (48), were kindly provided by David A. Fidock (Columbia University Medical Center, New York, NY).

Inhibitor pulse assay. The inhibitor pulse assay employed in this study to estimate LD_{50} and V_{min} have been described previously (45–47). Briefly, DHA, dAPC-S, and dAPC-L were serially diluted in CCM in 96-well v-bottom plates. Parasite culture was added to wells containing inhibitor (0.2% hematocrit [ht], 1% pt) and incubated for 3 h. Cells were washed four times with 200 μL CCM and incubated under standard conditions until assessment of parasitemia. Parasite viability following an inhibitor pulse is defined as the fraction of the parasite population that survives inhibitor exposure and is able to enter the next parasite cycle. Viability was determined by measuring the parasitemia in the parasite cycle following the inhibitor pulse. For this, parasites were fluorescently labeled with the RNA-binding dye, SYTO61, and the parasitemia was quantitated by flow cytometry. Viability was calculated in relation to parasitemia in the "untreated parasite" control (parasites not exposed to inhibitor) and "kill" control

cultures. The latter refers to parasites maintained under constant inhibitor pressure (>100 times the $LD_{50\_48\ h}$ for 48 to 96 h) to ensure quantitative killing of parasites. LD_{50} is the inhibitor concentration producing 50% viability. V_{min} is defined as the viability at saturating inhibitor concentration and was established by examining viability at the highest inhibitor concentration employed in a particular assay.

Modified inhibitor wash protocol. An inhibitor wash efficiency study was carried out as described previously (47). Briefly, 200-μL aliquots of uninfected RBCs (0.1% ht) in CCM were dispensed in 96-well v-bottom plates. Inhibitor (0 to 1 μM) was applied to wells, and cell suspensions were maintained for 3 h under standard culture conditions. Inhibitor was removed by washing the uninfected RBCs in CCM (4×) and were either maintained in the original plate (standard protocol, no transfer) or transferred (modified protocol) to a fresh plate. Cam3.II^{rev}-infected RBCs were aliquoted into wells containing washed uninfected RBCs (0.2% ht, ~1% pt). The culture was maintained until the next cycle, when parasite viability was assessed.

Stability studies. Inhibitor stability in different media was assessed as follows. Compound (100 μM) was incubated in PBS (pH 7.4), PBS (pH 7.4) + 10% plasma, CCM, and CCM + 10% plasma for various time periods before remnant activity was assessed. Similarly, inhibitor stability was examined in the presence of RBCs. Compound (100 μM) was incubated in the presence of RBCs (0.1, 1, and 10% ht in PBS) over various time periods. Remnant inhibitor activity was evaluated by exposing Cam3.II^{rev} parasites (25 to 30 h p.i.) to inhibitor (in serial dilution) for 3 h (26). The culture was maintained until the next cycle, when parasite viability was assessed.

Polyubiquitination and eIF2α phosphorylation. Protein ubiquitination and phosphorylation of eIF2α (P-eIF2α) were determined as previously described (10). Briefly, Cam3.II^{rev}-infected (25 to 30 h p.i.) RBCs (1 mL, 4 to 5% pt, 3% ht) were exposed to inhibitor or carrier in 24-well plates for 1.5 h for polyubiquitin detection, as per a previous report (26), or 3 h for P-eIF2α detection, to match the period of the protein translation assay (see below). The infected RBCs were pelleted at 380 × *g* for 5 min, resuspended in 500 μL PBS (+ cOmplete), and repelleted. Pelleted RBCs were lysed by resuspension in 500 μL PBS, cOmplete, and 0.05% saponin for 2 min at room temperature. Lysed RBCs were centrifuged at 380 × *g* for 10 min at 4°C. Pellets were washed 3 times in 200 μL PBS (+ cOmplete) and solubilized in Bolt LDS sample buffer containing reducing agent. Samples were resolved by SDS-PAGE (Bolt Bis-Tris 4 to 12% polyacrylamide gel, MES running buffer) and transferred (iBlot, Thermo Fisher Scientific) to nitrocellulose membranes. Membranes were blocked in mPBST (PBS supplemented with 3% wt/vol skim milk powder and 0.1% Tween 20) for 1 h at room temperature and probed with antiubiquitin (1:2,000), anti-P-eIF2α (1:500), and anti-*Pf*BiP (1:1,000) overnight at 4°C. Membranes were incubated with secondary antibody for 1 h at room temperature. The secondary antibodies were goat anti-rabbit IgG-peroxidase (for antiubiquitin and anti-P-eIF2α, 1:25,000) and goat anti-mouse IgG-peroxidase (for anti-*Pf*BiP, 1:25,000). Washed immunoblots were incubated with enhanced chemiluminescent (ECL) reagents before being imaged using the ChemiDoc MP imaging system (Bio-Rad, Hercules, CA).

Protein translation assay. Protein translation efficiency was estimated by incorporation of *O*-propargyl-puromycin (OPP), based on a method modified from previous reports (63, 64). Briefly, duplicate aliquots (200 μL) of Cam3.II^{rev}-infected RBCs (25 to 30 h p.i.; 0.2% ht and 1% pt) were treated with DHA, dAPC, and dAPC-L for 1 h in 96-well v-bottom plates. OPP solution (0.4 μL of 2 mM stock) was added and incubated for 2 h. Cells were washed 3 times in PBS and fixed in 4% formaldehyde and 0.02% glutaraldehyde (200 μL) for 30 min at room temperature. The cells were washed 3 times in PBS and 3% plasma and permeabilized in PBS, 3% plasma, and 0.05% Triton X-100 (200 μL) for 5 min at room temperature. Cells were fluorescently labeled by incubation in 200 μL reaction mix (PBS, 0.1 mM $CuSO_4$, 0.5 mM THPTA, 5 mM sodium ascorbate, and 0.1 μM Alexa Fluor 488 azide) for 1 h at 37°C. Cells were washed 4 times in PBS and 3% plasma and resuspended in PBS, 3% plasma, and 5 μg/mL propidium iodide (PI) (200 μL). Cells were incubated for 10 min at room temperature. Fluorescence was measured by flow cytometry (FACS Canto II; BD Biosciences, San Jose, CA).

SUPPLEMENTAL MATERIAL

Supplemental material is available online only.

SUPPLEMENTAL FILE 1, PDF file, 1 MB.

ACKNOWLEDGMENTS

We thank Daniel Barry, Tanya Puhalovich, Dean Andrew, Shannon Kenny, and David Gillett for technical support with cellular work and Alan Cowman for antibodies. We thank Yee-Foong Mok, Melbourne Protein Facility, for access to facilities. We acknowledge the facilities at the Ian Holmes Imaging Centre at Bio21 Institute (The University of Melbourne). We thank Stanley Xie for helpful discussions. We thank Dovile Anderson and the Monash Proteomics and Metabolomics Facility for high resolution LCMS.

We thank the Australian National Health and Medical Research Council for research support. L.T. was supported by an Australian Research Council Laureate Fellowship. X.L. is thankful for the support of a National Science and Technology Major Project for New Drug Development, China (2017ZX09101002-001-004) for R&D of dimeric artesunate glycerophosphocholine conjugate (dAPC). Y.D. received funding from the China

Scholarship Council (CSC) Program (201806090185) for a study period at the University of Melbourne.

REFERENCES

1. World Health Organisation. 2021. World malaria report 2021. https://www.who.int/teams/global-malaria-programme/reports/world-malaria-report-2021.
2. White NJ, Pukrittayakamee S, Hien TT, Faiz MA, Mokuolu OA, Dondorp AM. 2014. Malaria. Lancet 383:723–735. https://doi.org/10.1016/S0140-6736(13)60024-0.
3. O'Neill PM, Barton VE, Ward SA. 2010. The molecular mechanism of action of artemisinin: the debate continues. Molecules 15:1705–1721. https://doi.org/10.3390/molecules15031705.
4. Klonis N, Creek DJ, Tilley L. 2013. Iron and heme metabolism in *Plasmodium falciparum* and the mechanism of action of artemisinins. Curr Opin Microbiol 16:722–727. https://doi.org/10.1016/j.mib.2013.07.005.
5. Denisov E. 2011. An important role of intramolecular free radical reactions in antimalarial activity of artemisinin and its analogs. Org Biomol Chem 9:4219–4225. https://doi.org/10.1039/c0ob01150a.
6. Chen MZ, Moily NS, Bridgford JL, Wood RJ, Radwan M, Smith TA, Song Z, Tang BZ, Tilley L, Xu X, Reid GE, Pouladi MA, Hong Y, Hatters DM. 2017. A thiol probe for measuring unfolded protein load and proteostasis in cells. Nat Commun 8:11. https://doi.org/10.1038/s41467-017-00203-5.
7. Ismail HM, Barton V, Phanchana M, Charoensutthivarakul S, Wong MHL, Hemingway J, Biagini GA, O'Neill PM, Ward SA. 2016. Artemisinin activity-based probes identify multiple molecular targets within the asexual stage of the malaria parasites *Plasmodium falciparum* 3D7. Proc Natl Acad Sci U S A 113:2080–2085. https://doi.org/10.1073/pnas.1600459113.
8. Fügi MA, Wittlin S, Dong Y, Vennerstrom JL. 2010. Probing the antimalarial mechanism of artemisinin and OZ277 (arterolane) with nonperoxidic isosteres and nitroxyl radicals. Antimicrob Agents Chemother 54:1042–1046. https://doi.org/10.1128/AAC.01305-09.
9. Li J, Zhou B. 2010. Biological actions of artemisinin: insights from medicinal chemistry studies. Molecules 15:1378–1397. https://doi.org/10.3390/molecules15031378.
10. Bridgford JL, Xie SC, Cobbold SA, Pasaje CFA, Herrmann S, Yang T, Gillett DL, Dick LR, Ralph SA, Dogovski C, Spillman NJ, Tilley L. 2018. Artemisinin kills malaria parasites by damaging proteins and inhibiting the proteasome. Nat Commun 9:3801. https://doi.org/10.1038/s41467-018-06221-1.
11. Giannangelo C, Siddiqui G, De Paoli A, Anderson BM, Edgington-Mitchell LE, Charman SA, Creek DJ. 2020. System-wide biochemical analysis reveals ozonide antimalarials initially act by disrupting *Plasmodium falciparum* haemoglobin digestion. PLoS Pathog 16:e1008485. https://doi.org/10.1371/journal.ppat.1008485.
12. Karbwang J, Na-Bangchang K, Congpuong K, Molunto P, Thanavibul A. 1997. Pharmacokinetics and bioavailability of oral and intramuscular artemether. Eur J Clin Pharmacol 52:307–310. https://doi.org/10.1007/s002280050295.
13. Li QG, Peggins JO, Fleckenstein LL, Masonic K, Heiffer MH, Brewer TG. 1998. The pharmacokinetics and bioavailability of dihydroartemisinin, arteether, artemether, artesunic acid and artelinic acid in rats. J Pharm Pharmacol 50:173–182. https://doi.org/10.1111/j.2042-7158.1998.tb06173.x.
14. Hien TT, Davis TM, Chuong LV, Ilett KF, Sinh DX, Phu NH, Agus C, Chiswell GM, White NJ, Farrar J. 2004. Comparative pharmacokinetics of intramuscular artesunate and artemether in patients with severe falciparum malaria. Antimicrob Agents Chemother 48:4234–4239. https://doi.org/10.1128/AAC.48.11.4234-4239.2004.
15. Newton P, Suputtamongkol Y, Teja-Isavadharm P, Pukrittayakamee S, Navaratnam V, Bates I, White N. 2000. Antimalarial bioavailability and disposition of artesunate in acute falciparum malaria. Antimicrob Agents Chemother 44:972–977. https://doi.org/10.1128/AAC.44.4.972-977.2000.
16. Ansari MT, Saify ZS, Sultana N, Ahmad I, Saeed-Ul-Hassan S, Tariq I, Khanum M. 2013. Malaria and artemisinin derivatives: an updated review. Mini Rev Med Chem 13:1879–1902. https://doi.org/10.2174/13895575113136660097.
17. Li X-Q, Björkman A, Andersson TB, Gustafsson LL, Masimirembwa CM. 2003. Identification of human cytochrome P(450)s that metabolise antiparasitic drugs and predictions of *in vivo* drug hepatic clearance from *in vitro* data. Eur J Clin Pharmacol 59:429–442. https://doi.org/10.1007/s00228-003-0636-9.
18. Wang J, Xu C, Liao FL, Jiang T, Krishna S, Tu Y. 2019. A temporizing solution to "artemisinin resistance". N Engl J Med 380:2087–2089. https://doi.org/10.1056/NEJMp1901233.
19. Amaratunga C, Lim P, Suon S, Sreng S, Mao S, Sopha C, Sam B, Dek D, Try V, Amato R, Blessborn D, Song L, Tullo GS, Fay MP, Anderson JM, Tarning J, Fairhurst RM. 2016. Dihydroartemisinin–piperaquine resistance in *Plasmodium falciparum* malaria in Cambodia: a multisite prospective cohort study. Lancet Infect Dis 16:357–365. https://doi.org/10.1016/S1473-3099(15)00487-9.
20. van der Pluijm RW, Imwong M, Chau NH, Hoa NT, Thuy-Nhien NT, Thanh NV, Jittamala P, Hanboonkunupakarn B, Chutasmit K, Saelow C, Runjarern R, Kaewmok W, Tripura R, Peto TJ, Yok S, Suon S, Sreng S, Mao S, Oun S, Yen S, Amaratunga C, Lek D, Huy R, Dhorda M, Chotivanich K, Ashley EA, Mukaka M, Waithira N, Cheah PY, Maude RJ, Amato R, Pearson RD, Gonçalves S, Jacob CG, Hamilton WL, Fairhurst RM, Tarning J, Winterberg M, Kwiatkowski DP, Pukrittayakamee S, Hien TT, Day NPJ, Miotto O, White NJ, Dondorp AM. 2019. Determinants of dihydroartemisinin-piperaquine treatment failure in *Plasmodium falciparum* malaria in Cambodia, Thailand, and Vietnam: a prospective clinical, pharmacological, and genetic study. Lancet Infectious Diseases 19:952–961. https://doi.org/10.1016/S1473-3099(19)30391-3.
21. Ariey F, Witkowski B, Amaratunga C, Beghain J, Langlois AC, Khim N, Kim S, Duru V, Bouchier C, Ma L, Lim P, Leang R, Duong S, Sreng S, Suon S, Chuor CM, Bout DM, Menard S, Rogers WO, Genton B, Fandeur T, Miotto O, Ringwald P, Le Bras J, Berry A, Barale JC, Fairhurst RM, Benoit-Vical F, Mercereau-Puijalon O, Menard D. 2014. A molecular marker of artemisinin-resistant *Plasmodium falciparum* malaria. Nature 505:50–55. https://doi.org/10.1038/nature12876.
22. Uwimana A, Legrand E, Stokes BH, Ndikumana JM, Warsame M, Umulisa N, Ngamije D, Munyaneza T, Mazarati JB, Munguti K, Campagne P, Criscuolo A, Ariey F, Murindahabi M, Ringwald P, Fidock DA, Mbituyumuremyi A, Menard D. 2020. Emergence and clonal expansion of in vitro artemisinin-resistant *Plasmodium falciparum* kelch13 R561H mutant parasites in Rwanda. Nat Med 26:1602–1608. https://doi.org/10.1038/s41591-020-1005-2.
23. Yang T, Yeoh LM, Tutor MV, Dixon MW, McMillan PJ, Xie SC, Bridgford JL, Gillett DL, Duffy MF, Ralph SA, McConville MJ, Tilley L, Cobbold SA. 2019. Decreased K13 abundance reduces hemoglobin catabolism and proteotoxic stress, underpinning artemisinin resistance. Cell Rep 29:2917–2928.e5. https://doi.org/10.1016/j.celrep.2019.10.095.
24. Birnbaum J, Scharf S, Schmidt S, Jonscher E, Hoeijmakers WAM, Flemming S, Toenhake CG, Schmitt M, Sabitzki R, Bergmann B, Frohlke U, Mesen-Ramirez P, Blancke Soares A, Herrmann H, Bartfai R, Spielmann T. 2020. A Kelch13-defined endocytosis pathway mediates artemisinin resistance in malaria parasites. Science 367:51–59. https://doi.org/10.1126/science.aax4735.
25. Siddiqui G, Srivastava A, Russell AS, Creek DJ. 2017. Multi-omics based identification of specific biochemical changes associated with PfKelch13-mutant artemisinin-resistant *Plasmodium falciparum*. J Infect Dis 215:1435–1444. https://doi.org/10.1093/infdis/jix156.
26. Dogovski C, Xie SC, Burgio G, Bridgford J, Mok S, McCaw JM, Chotivanich K, Kenny S, Gnadig N, Straimer J, Bozdech Z, Fidock DA, Simpson JA, Dondorp AM, Foote S, Klonis N, Tilley L. 2015. Targeting the cell stress response of *Plasmodium falciparum* to overcome artemisinin resistance. PLoS Biol 13:e1002132. https://doi.org/10.1371/journal.pbio.1002132.
27. Giannangelo C, Fowkes FJI, Simpson JA, Charman SA, Creek DJ. 2019. Ozonide antimalarial activity in the context of artemisinin-resistant malaria. Trends Parasitol 35:529–543. https://doi.org/10.1016/j.pt.2019.05.002.
28. Gabizon A, Papahadjopoulos D. 1988. Liposome formulations with prolonged circulation time in blood and enhanced uptake by tumors. Proc Natl Acad Sci U S A 85:6949–6953. https://doi.org/10.1073/pnas.85.18.6949.
29. Rana N, Cultrara C, Phillips M, Sabatino D. 2017. Functionalization of peptide nucleolipid bioconjugates and their structure anti-cancer activity relationship studies. Bioorg Med Chem Lett 27:4019–4023. https://doi.org/10.1016/j.bmcl.2017.07.056.
30. Green AE, Rose PG. 2006. Pegylated liposomal doxorubicin in ovarian cancer. Int J Nanomedicine 1:229–239.
31. Meerum Terwogt JM, ten Bokkel Huinink WW, Schellens JH, Schot M, Mandjes IA, Zurlo MG, Rocchetti M, Rosing H, Koopman FJ, Beijnen JH. 2001. Phase I clinical and pharmacokinetic study of PNU166945, a novel

water-soluble polymer-conjugated prodrug of paclitaxel. Anticancer Drugs 12:315–323. https://doi.org/10.1097/00001813-200104000-00003.
32. Pelt J, Busatto S, Ferrari M, Thompson EA, Mody K, Wolfram J. 2018. Chloroquine and nanoparticle drug delivery: a promising combination. Pharmacol Ther 191:43–49. https://doi.org/10.1016/j.pharmthera.2018.06.007.
33. Gabriels M, Plaizier-Vercammen J. 2003. Physical and chemical evaluation of liposomes, containing artesunate. J Pharm Biomed Anal 31:655–667. https://doi.org/10.1016/s0731-7085(02)00678-7.
34. Kumar H, Gothwal A, Khan I, Nakhate KT, Alexander A, Ajazuddin Singh V, Gupta U. 2017. Galactose-anchored gelatin nanoparticles for primaquine delivery and improved pharmacokinetics: a biodegradable and safe approach for effective antiplasmodial activity against *P falciparum* 3D7 and in vivo hepatocyte targeting. Mol Pharm 14:3356–3369. https://doi.org/10.1021/acs.molpharmaceut.7b00376.
35. Righeschi C, Coronnello M, Mastrantoni A, Isacchi B, Bergonzi MC, Mini E, Bilia AR. 2014. Strategy to provide a useful solution to effective delivery of dihydroartemisinin: development, characterization and in vitro studies of liposomal formulations. Colloids Surf B Biointerfaces 116:121–127. https://doi.org/10.1016/j.colsurfb.2013.12.019.
36. Crommelin DJ, Storm G. 2003. Liposomes: from the bench to the bed. J Liposome Res 13:33–36. https://doi.org/10.1081/lpr-120017488.
37. Kapoor M, Lee SL, Tyner KM. 2017. Liposomal drug product development and quality: current US experience and perspective. AAPS J 19:632–641. https://doi.org/10.1208/s12248-017-0049-9.
38. He H, Lu Y, Qi J, Zhu Q, Chen Z, Wu W. 2019. Adapting liposomes for oral drug delivery. Acta Pharm Sin B 9:36–48. https://doi.org/10.1016/j.apsb.2018.06.005.
39. Fang S, Hou Y, Ling L, Wang D, Ismail M, Du Y, Zhang Y, Yao C, Li X. 2018. Dimeric camptothecin derived phospholipid assembled liposomes with high drug loading for cancer therapy. Colloids Surf B Biointerfaces 166:235–244. https://doi.org/10.1016/j.colsurfb.2018.02.046.
40. Du Y, Zhang W, He R, Ismail M, Ling L, Yao C, Fu Z, Li X. 2017. Dual 7-ethyl-10-hydroxycamptothecin conjugated phospholipid prodrug assembled liposomes with in vitro anticancer effects. Bioorg Med Chem 25:3247–3258. https://doi.org/10.1016/j.bmc.2017.04.025.
41. He W, Du Y, Zhou W, Yao C, Li X. 2019. Redox-sensitive dimeric camptothecin phosphatidylcholines-based liposomes for improved anticancer efficacy. Nanomedicine (Lond) 14:3057–3074. https://doi.org/10.2217/nnm-2019-0261.
42. Ismail M, Ling L, Du Y, Yao C, Li X. 2018. Liposomes of dimeric artesunate phospholipid: a combination of dimerization and self-assembly to combat malaria. Biomaterials 163:76–87. https://doi.org/10.1016/j.biomaterials.2018.02.026.
43. Zhang Y, He W, Du Y, Du Y, Zhao C, Zhang Y, Zhang H, Yin L, Li X. 2020. Dimeric artesunate phospholipid-conjugated liposomes as promising anti-inflammatory therapy for rheumatoid arthritis. Int J Pharm 579:119178. https://doi.org/10.1016/j.ijpharm.2020.119178.
44. Jansen FH, Soomro SA. 2007. Chemical instability determines the biological action of the artemisinins. Curr Med Chem 14:3243–3259. https://doi.org/10.2174/092986707782793844.
45. Klonis N, Xie SC, McCaw JM, Crespo-Ortiz MP, Zaloumis SG, Simpson JA, Tilley L. 2013. Altered temporal response of malaria parasites determines differential sensitivity to artemisinin. Proc Natl Acad Sci U S A 110:5157–5162. https://doi.org/10.1073/pnas.1217452110.
46. Xie SC, Dogovski C, Kenny S, Tilley L, Klonis N. 2014. Optimal assay design for determining the in vitro sensitivity of ring stage *Plasmodium falciparum* to artemisinins. Int J Parasitol 44:893–899. https://doi.org/10.1016/j.ijpara.2014.07.008.
47. Yang T, Xie SC, Cao P, Giannangelo C, McCaw J, Creek DJ, Charman SA, Klonis N, Tilley L. 2016. Comparison of the exposure time dependence of the activities of synthetic ozonide antimalarials and dihydroartemisinin against K13 wild-type and mutant *Plasmodium falciparum* strains. Antimicrob Agents Chemother 60:4501–4510. https://doi.org/10.1128/AAC.00574-16.
48. Straimer J, Gnadig NF, Witkowski B, Amaratunga C, Duru V, Ramadani AP, Dacheux M, Khim N, Zhang L, Lam S, Gregory PD, Urnov FD, Mercereau-Puijalon O, Benoit-Vical F, Fairhurst RM, Menard D, Fidock DA. 2015. K13-propeller mutations confer artemisinin resistance in *Plasmodium falciparum* clinical isolates. Science 347:428–431. https://doi.org/10.1126/science.1260867.
49. Lindegardh N, Hanpithakpong W, Kamanikom B, Singhasivanon P, Socheat D, Yi P, Dondorp AM, McGready R, Nosten F, White NJ, Day NP. 2008. Major pitfalls in the measurement of artemisinin derivatives in plasma in clinical studies. J Chromatogr B Analyt Technol Biomed Life Sci 876:54–60. https://doi.org/10.1016/j.jchromb.2008.10.021.
50. Parapini S, Olliaro P, Navaratnam V, Taramelli D, Basilico N. 2015. Stability of the antimalarial drug dihydroartemisinin under physiologically relevant conditions: implications for clinical treatment and pharmacokinetic and *in vitro* assays. Antimicrob Agents Chemother 59:4046–4052. https://doi.org/10.1128/AAC.00183-15.
51. Haynes RK, Chan HW, Lung CM, Ng NC, Wong HN, Shek LY, Williams ID, Cartwright A, Gomes MF. 2007. Artesunate and dihydroartemisinin (DHA): unusual decomposition products formed under mild conditions and comments on the fitness of DHA as an antimalarial drug. ChemMedChem 2:1448–1463. https://doi.org/10.1002/cmdc.200700064.
52. Giannangelo C, Stingelin L, Yang T, Tilley L, Charman SA, Creek DJ. 2018. Parasite-mediated degradation of synthetic ozonide antimalarials impacts *in vitro* antimalarial activity. Antimicrob Agents Chemother 62:e01566-17. https://doi.org/10.1128/AAC.01566-17.
53. Hughes D, Mallucci GR. 2019. The unfolded protein response in neurodegenerative disorders – therapeutic modulation of the PERK pathway. FEBS J 286:342–355. https://doi.org/10.1111/febs.14422.
54. Uttamapinant C, Sanchez MI, Liu DS, Yao JZ, White KA, Grecian S, Clark S, Gee KR, Ting AY. 2013. Site-specific protein labeling using PRIME and chelation-assisted click chemistry. Nat Protoc 8:1620–1634. https://doi.org/10.1038/nprot.2013.096.
55. Bunjes H, Rades T. 2005. Thermotropic liquid crystalline drugs. J Pharm Pharmacol 57:807–816. https://doi.org/10.1211/0022357056208.
56. Tilley L, Charman SA, Vennerstrom JL. 2011. Semisynthetic artemisinin and synthetic peroxide antimalarials, p 33–64. *In* Palmer MJ, Wells TNC (ed), RSC drug discovery series: neglected diseases and drug discovery. RSC Publishing, London, UK.
57. Creek DJ, Chiu FC, Prankerd RJ, Charman SA, Charman WN. 2005. Kinetics of iron-mediated artemisinin degradation: effect of solvent composition and iron salt. J Pharm Sci 94:1820–1829. https://doi.org/10.1002/jps.20400.
58. Wu W-M, Wu Y, Wu Y-L, Yao Z-J, Zhou C-M, Li Y, Shan F. 1998. Unified mechanistic framework for the Fe(II)-induced cleavage of Qinghaosu and derivatives/analogues. The first spin-trapping evidence for the previously postulated secondary C-4 radical. J Am Chem Soc 120:3316–3325. https://doi.org/10.1021/ja973080o.
59. Cao P, Klonis N, Zaloumis S, Dogovski C, Xie SC, Saralamba S, White LJ, Fowkes FJI, Tilley L, Simpson JA, McCaw JM. 2017. A dynamic stress model explains the delayed drug effect in artemisinin treatment of *Plasmodium falciparum*. Antimicrob Agents Chemother 61:e00618-17. https://doi.org/10.1128/AAC.00618-17.
60. Creek DJ, Ryan E, Charman WN, Chiu FC, Prankerd RJ, Vennerstrom JL, Charman SA. 2009. Stability of peroxide antimalarials in the presence of human hemoglobin. Antimicrob Agents Chemother 53:3496–3500. https://doi.org/10.1128/AAC.00363-09.
61. Vennerstrom JL, Arbe-Barnes S, Brun R, Charman SA, Chiu FC, Chollet J, Dong Y, Dorn A, Hunziker D, Matile H, McIntosh K, Padmanilayam M, Santo Tomas J, Scheurer C, Scorneaux B, Tang Y, Urwyler H, Wittlin S, Charman WN. 2004. Identification of an antimalarial synthetic trioxolane drug development candidate. Nature 430:900–904. https://doi.org/10.1038/nature02779.
62. Dong Y, Chollet J, Matile H, Charman SA, Chiu FC, Charman WN, Scorneaux B, Urwyler H, Santo Tomas J, Scheurer C, Snyder C, Dorn A, Wang X, Karle JM, Tang Y, Wittlin S, Brun R, Vennerstrom JL. 2005. Spiro and dispiro-1,2,4-trioxolanes as antimalarial peroxides: charting a workable structure-activity relationship using simple prototypes. J Med Chem 48:4953–4961. https://doi.org/10.1021/jm049040u.
63. Uttamapinant C, Tangpeerachaikul A, Grecian S, Clarke S, Singh U, Slade P, Gee KR, Ting AY. 2012. Fast, cell-compatible click chemistry with copper-chelating azides for biomolecular labeling. Angew Chem Int Ed Engl 51:5852–5856. https://doi.org/10.1002/anie.201108181.
64. Presolski SI, Hong VP, Finn MG. 2011. Copper-catalyzed azide-alkyne click chemistry for bioconjugation. Curr Protoc Chem Biol 3:153–162. https://doi.org/10.1002/9780470559277.ch110148.